REPORT DOCUMENTATION PAGE

Form Approved

OMB No. 0704-0188

1. REPORT DATE *(DD-MM-YYYY)*	2. REPORT TYPE	3. DATES COVERED *(From - To)*
07-09-2015	Final	19 March 2013 to 18 March 2015

4. TITLE AND SUBTITLE

Thermoelectric transducer using bio nano process

5a. CONTRACT NUMBER
FA2386-13-1-4061

5b. GRANT NUMBER
Grant 13RSZ052_134061

5c. PROGRAM ELEMENT NUMBER
61102F

6. AUTHOR(S)

Prof Yukiharu Uraoka

5d. PROJECT NUMBER

5e. TASK NUMBER

5f. WORK UNIT NUMBER

7. PERFORMING ORGANIZATION NAME(S) AND ADDRESS(ES)
Nara Institute of Science and Technology
8916-5, Takayama, Ikoma, Nara
Nara 630-0192
Japan

8. PERFORMING ORGANIZATION REPORT NUMBER

N/A

9. SPONSORING/MONITORING AGENCY NAME(S) AND ADDRESS(ES)

AOARD
UNIT 45002
APO AP 96338-5002

10. SPONSOR/MONITOR'S ACRONYM(S)

AFRL/AFOSR/IOA(AOARD)

11. SPONSOR/MONITOR'S REPORT NUMBER(S)
13RSZ052_134061

12. DISTRIBUTION/AVAILABILITY STATEMENT

Distribution Code A: Approved for public release, distribution is unlimited.

13. SUPPLEMENTARY NOTES

14. ABSTRACT

As an application to thermos transducer, bio nano process was developed. Distance controlled nanoparticles (NPs) array was investigated using a simple spin coating process. It was found that the separation distance of NPs was controlled at the nanoscale by using Poly-Ethylene Glycols (PEGs).

15. SUBJECT TERMS

Nano-Materials, nano-bio, Thermoelectric

16. SECURITY CLASSIFICATION OF:			17. LIMITATION OF ABSTRACT	18. NUMBER OF PAGES	19a. NAME OF RESPONSIBLE PERSON
a. REPORT	b. ABSTRACT	c. THIS PAGE			Seng Hong, Ph.D.
U	U	U	SAR	24	**19b. TELEPHONE NUMBER** *(Include area code)* +81-42-511-2000

Final Report (AOARD134061)

August 1, 2015

Thermoelectric transducer using bio nano process

Yukiharu Uraoka

Graduate School of Material Science Nara Institute of Science and Technology

8916-5 Takayama, Ikoma, Nara 630-0192, Japan

uraoka@ms.naist.jp.

KEYWORDS: Ferritin; Thermal Transducer; Nanoparticle; Ammonium acetate; Separation distance; Debye length.

ABSTRACT: As an application to thermos transducer, bio nano process was developed. Distance controlled nanoparticles (NPs) array was investigated using a simple spin coating process. It was found that the separation distance of NPs was controlled at the nanoscale by using Poly-Ethylene Glycols (PEGs). Ferritin was used to synthesize NPs and carry them to a substrate by using the different molecular weight of PEGs. In order to control the distance of the NPs, PEGs with molecular weights of 2k, 5k, 10k and 20k were modified on ferritin with 10 mM ion strength and 0.01 mg/ml

ferritin concentration. The separated distances of NPs increased along with increase in PEG molecular weight. BiTeSb thin film embedded with ferritin nano particle were fabricated and Seebeck coefficient and sheet resistance were evaluated. Power factor was enhanced by 20% with high density of NPs due to de-dopping and energy filtering effect.

Introduction

Nanoparticles (NPs) have great potential to be used as components in nanotechnology. There are many applications such as solar cell devices[1], memory[2], laser[3] and new materials' manufacture[4-6]. In most devices, NPs are arrayed on the solid surface as a first step. The NPs and their separated distance (SD), which has been defined as the distance from the center of a NP to another's, play important roles in nano-composite structure. Especially, in thermoelectric materials, the SD and diameter of NP are important factor to increase an efficiency. As we known, figure of merit (ZT value) in thermoelectric devise increase to introduce nanostructures into thermoelectric materials[7]. Among all the nanostructures, thin film with inserting NPs in matrix has been proved an excellent way to improve properties of thermoelectric materials[8, 9, 10]. Through theoretical results about NPs radius from Y. Ezzahri, it is known that NPs in around 7 nm diameter are very useful to scatter phonon at room temperature[11]. Additionally, SD of nanostructure must be designed in order to scatter phonon but not effect electron diffusion. In Bi_2Te_3 material, phonon and electron mean free path are around 100 nm

and 30 nm, respectively. Thus, SD must be set around 40 nm to reduce a thermal conductivity effectively.

Many methods to produce the NP array have been researched for various applications[12-18]. Physical and chemical methods are being developing for improvement of NPs' fabrication and distribution. However, these methods poorly control the size and distribution at the nanoscale. Therefore, a biological method has been investigated to synthesize NPs due to uniformity at nanoscale[19]. This method, which is called the Bio Nano Process (BNP), was introduced for device applications[20]. As the basic tool of BNP, the ferritin protein molecule has been studied. Ferritin, which consists of 24 polypeptide subunits, is a spherical cage protein with inner and outer diameters of 7 nm and 12 nm, respectively[21, 22]. The BNP was developed to form an array of ferritin with homogeneous NP on a SiO_2 surface. Additionally, an independent NP array is produced after elimination of the protein shell[23–28]. Several researches have investigated adsorption mechanisms of ferritin on substrates[29–35].

PEG-ferritin (ferritin modified by polyethylene glycol) was synthesized by first using Fer8 and PEG. Fer0 consists of all L-type ferritin sub-unites[36, 37]. On the other hand, Fer8 is a structure in which 8 amino acid residues have been removed from all consisted base pairs along the N-terminal direction[38, 39]. Because of this change, Fer8 surface shows negative charge and Fer8 is easily modified by the PEG.

In the BNP, NPs distribution method with conditions of protein concentration, ion strength and PEG weight has been researched for optimization of foundational conditions. The relationship between the conditions and array of NPs has been

discussed[40]. Furthermore, through measurement of PEG-ferritin diameter and simulation of adsorption, the mechanism of ferritin adsorption on SiO_2 surface has been reported[40]. The PEG modification is a useful method to make a gap between NPs. However, a comprehensive understanding of the controllability of SD is still lacking and a method for controlling SD should be researched based on analysis by calculation of NP density. The mean value for distribution of NPs is just a rough analysis and difficult to figure out the actual distances. Therefore, a different method to evaluate the distribution of SDs is required. In this research, the controllability of SD by using PEG was evaluated. In order to control the SD and analyze distribution of SD, different molecular weights of PEGs were modified on ferritin and all the SDs between PEG-ferritins calculated for analyzing the distribution in detail. The SD distribution was evaluated by using radial distribution function (RDF) and FWHM of histograms. In RDF calculation, every distance between two NPs is calculated and the numbers of NPs is counted using scanning electron microscope (SEM) images.

Preparation and Evaluation of PEG-ferritin

The lysine residues on the surface of ferritin were reacted with PEG succinimide ester (Meo-PEG-NHS). At first, the detail of experimental protocol is mass designed amount of MeO-PEG-NHS per subunit of ferritin in a falcon tube, then the powder of Meo-PEG-NHS is dissolved in 5.0 mL 100 mM Tris-HCl buffer (pH = 8.2) which is filtrated by 0.20 μm membrane filter (ADVANTEC, DISMIC-25CS). Next, Fer8 (1.0 mg) which was completed with biomineralization of the iron core (Fig. 1(a)) after

dissolving in 100 mM Tris-HCl buffer (pH = 8.2) and PEG derivative solution was pre-prepared at first, were mixed in order to adjust final concentration of ferritin to 0.2 mg/ml. Finally, at a temperature of 4 ^{o}C, the reaction solution is left in a dark place for 60 hours.

In this experiment, PEG molecular weights 2k, 5k, 10k and 20k were modified on ferritin. In order to study the number of modified PEGs on one ferritin sub-unit, the synthesized PEG-ferritins (Fig. 1(b)) were analyzed by matrix assisted laser desorption ionization time-of-flight mass spectrometry (MALDI-TOF/MS). Additionally, diameters of PEG-ferritin in solution were calculated by dynamic light scattering (DLS) measurement. The measurement conditions of DLS were: protein density 0.2 mg/ml, and NaCl solution concentration of 10 mM. MALDI-TOF/MS results are shown in Fig. 2. Molecular weight of one ferritin sub-unit is 19 kDa. Therefore, the MALDI-TOF/MS result of apo-ferritin (without PEG modification) is identical with the theoretical value. If one PEG10k is successfully modified on a ferritin sub-unit, the molecular weight of this sub-unit increases 10k. From MALDI-TOF/MS results (Fig. 2), it is known that attachment of PEG2k for Fer8 sub-units about 44 % were modified two PEGs and about 56 % were modified three PEGs. That means almost 61 PEGs were modified on one ferritin. Furthermore, for other PEG molecular weights, around 39, 50 and 44 PEGs were modified on one ferritin with PEG5k, PEG10k and PEG20k, respectively. From Fig. 2, the numbers of modified PEGs on one ferritin indicate that the number of modified PEG mostly decreased along with increase in PEG molecular weight. We consider that foremost modified PEGs will obstruct additional modification. This effect should strengthen when PEG length becomes longer which means the utilization of

longer PEG will decrease number of PEG on ferritin. DLS results are shown in Fig. 3. As a reference, apo-ferritin was measured. The DLS results show that the diameter of apo-ferritin is 12.7 nm. DLS results for the ferritin with PEG2k, 5k, 10k and 20k are 17.0 nm, 24.6 nm, 35.8 nm and 45.2 nm, respectively. Therefore, the measured PEG thickness increased as the PEG molecular weight increased. From the theoretical calculation of PEG length, it was known that experiment values of PEG length are much shorter than calculated values. Thus, PEGs modified on ferritin are not in brush state in solution. That is, they twisted and twined around the ferritin. Therefore the modification of PEG will increase steric hindrance for the further modifications.

Experimental method

The concentration of buffer and ferritin were optimized before the experiment (supporting info.)[40]. Through repeating and developing the experiments, the density of adsorption and aggregation of ferritin were considered. As optimized conditions, ferritin concentration of 0.01 mg/ml and ammonium acetate (AA) ion concentration of 10 mM, were used in the experiment. The array of PEG-ferritin was formed in the following steps. At first, Si substrates with 3 nm thickness thermal oxide layer were cleaned by acetone and methanol to remove organic and inorganic contaminants. Then the samples were cleaned with pure water and dried with N_2. After the cleaning process, the samples were treated by UV-Ozone for 10 min at 115 ^{o}C in order to change hydrophobic into a hydrophilic surface. Then, the samples were put into pure water to store before the next step. After the spin dry process to remove the pure water, the PEG-ferritin with PEG

modification of 2k, 5k, 10k and 20k were dropped on the samples and held for 3 min. During this incubation time, PEG-ferritins adsorbed on to the SiO_2 surface. Then, the solution was removed utilizing the spin coater (first: 360 rpm in 30s, second: 1000 rpm in 60s and third: 3000 rpm in 30s). Finally, the NPs on the samples were observed using SEM to evaluate the relationship between SD and the molecular weight of PEG.

Results and Discussion

SEM images of NPs on the SiO_2 surface are shown in Fig. 4. The white dots in Fig. 4 are FeO_x NPs with diameter of 6 nm. In the SEM images of PEG2k-ferritin and PEG5k-ferritin, there were some aggregations. In contrast, PEG10k-ferritin and PEG20k-ferritin were evenly distributed on the SiO_2 surface. As shown in the SEM images, the NP density was decreased with an increase in the molecular weight of PEG. To analyze the distribution of NPs, RDF was introduced. RDF can be expressed as, $g(r) = N/(2\pi r\rho\Delta r)$, where N is the number of NPs in $2\pi r\Delta r$ area, r is distance from one NP, ρ is density of NPs[41]. Therefore $g(r)$ means the probability of finding a NP in the area of $2\pi r\Delta r$ at distance r. Because ρ is constant, it can be ignored in our calculation. Thus, the formula of $g'(r) = N/(2\pi r\Delta r)$ was used in our study. In the calculation, Δr was set at 1 nm. The calculated RDF using SEM images are shown in Fig. 5. The separation distances' peak shift to the longer direction along with increasing molecular weight of PEG. The first peak values (1st nearest distance) of PEG2k-ferritin, PEG5k-ferritin, PEG10k-ferritin and PEG20k-ferritin were 30 nm, 34 nm, 39 nm and 53 nm, respectively. Along with increasing the molecular weight, the second peak became

clear. This means that the array of NPs changed from a totally random to more order structure while longer PEGs are used. For analysis of statistical dispersion in the distribution of NPs, a histogram of SDs was calculated (Fig. 6). In this calculation, the central point of each NP was set as the NP position. The four nearest neighboring NP distances were measured. After calculation of the histogram, Gaussian function was used to fit the histogram and FWHMs were calculated as statistical dispersion of NPs distribution. The calculated SD (from RDF) and FWHM (from histogram) are plotted against PEG molecular weight in Fig. 7. The SD increases almost linearly with increasing PEG molecular weight. On the other hand, FWHM is almost constant against the PEG molecular weight. The FWHM value was limited within the region of about 15-20 nm. Narrow distribution of FWHM means a more uniform SD, and it should be very important for nano-composited material properties. Thus, not only SDs but also FWHM should be considered in order to fabricate nano-composite materials.

At the solution condition of 10 mM concentration, the Debye length of ferritin is shorter than 3 nm[40]. Comparing it with the DLS results (Fig. 3), the Debye length is almost equal to the thickness of the PEG2k layer in solution. The electrostatic interaction between ferritins is the main component for interaction of PEG2k-ferritin. Although this electrostatic interaction is a longer distance effect, it is not enough to control the separation distance precisely. If longer PEG than PEG2k is used with the same condition, the interaction of PEG should be a main effect to define the separation distance of ferritins. Therefore, PEG molecular weight is a critical factor for distribution of SDs. From the DLS results, it could be seen that the thicknesses of the PEG layers are 2.2 nm, 6.0 nm, 11.6 nm and 16.3 nm, respectively. On the other hand, the

calculated PEG thicknesses using the first peak value of RDF of PEG2k-20k are around 9 nm, 11 nm, 14 nm and 21 nm, respectively. Therefore, the same trend between RDF results and DLS results suggests that effective PEG length is a main factor to define the SD. But there are still differences, and PEG thickness from RDF results are larger than that of DLS results. This can be considered as unsaturated adsorption of PEG-ferritin or electrostatic interaction between PEG layers.

This method to control the distance of NP array could be applied on not only SiO_2 surface but also many metal or metal oxide surfaces. On other material surfaces, Zeta potential is a critical factor to form a NP array with controlled distance. Therefore, spin coating conditions are different with SiO_2 surface (Supporting Info.).

Next we fabricated BiTeSb film embedded with ferritin nano particle as shown in Fig.8. At first, 100 nm BiTeSb was deposited on sapphire substrate with Pulse Laser Deposition at 250 degrees. Then we removed outer protein by UV/Ozone treatment. Once again, 100 nm BiTeSb was deposited onto the nano particle. Finally samples were annealed with N_2 and H_2 ambient at 250 degree. And iron oxide were reduced to metal iron. In this experiment, 3 samples with non NPs, low and high density NP samples were prepared as shown in Fig.9. Then Seebeck coefficient and electrical resistance were evaluated as shown in Fig.10. From the comparison of different three density, we found that Seebeck coefficient and resistance greatly increased by incresing NPs.

Here we discuss the increase of Seebeck coefficient and decrease of conductivity. The change of Seebeck coefficient and conductivity by the introduction of the NP is considered to be due to the energy filtering effects and carrier de-dopping. The energy band diagram of this structure is shown in Fig.11. At the interface of iron and BiTeSb,

the carriers in BiTeSb go through NPs should get over potential barrier of approximately 0.6 eV. This barrier can filter out low energy electron to increase Seebeck coefficient. On the other hand, sheet resistance increased due to the carrier scattering of oxide NPs. Because the irons oxides were partially remained. Furthermore, BiTeSb is p-type semiconductor, and iron oxide NPs is also p-type semiconductor, so by embedding NPs, carrier de-dopping effect occured as shown in Fig.12. Thus power factor was enhanced by 20% with high density of NPs due to de-dopping and energy filtering effect.

Conclusion

A nanoparticle controllable array was successfully fabricated on SiO_2 and metal surface using different types of PEG-ferritin with a simple spin coating process. Through the results of MALDI-TOF/MS and DLS, the states of PEG-ferritin were studied. MALDI-TOF/MS results suggested that ferritin sub-units are modified on two or three PEGs, which have low molecular weight, but one or two PEGs. On the other hand, DLS results indicated that the diameter of PEG-ferritin increased with an increase in PEG molecular weight. In order to evaluate the SD, RDF and FWHM were calculated using SEM images. This calculation indicated that SDs increase along with increasing the PEG molecular weight. The exact control of NPs distribution is very useful for not only nano-composites materials but also device fabrication. Furthermore, the NPs materials can be changed to different materials. Thus a wide utilization of

materials could be used as NPs for nanotechnology and fabrication of devices. BiTeSb thin film embedded with ferritin nano particle were fabricated and Seebeck coefficient and sheet resistance were evaluated. Power factor was enhanced by 20% with high density of NPs due to de-dopping and energy filtering effect.

*S Supporting Information

With PEG2k ferritin (0.05 mg/ml), NP arrays were formed in the conditions of ammonium acetate buffer from 0 mM to 10 mM. From the results of SEM images (Fig. S1), it was suggested that the density of NPs adsorption increased along with increase of ammonium acetate concentration. Histograms were also calculated by using these SEM images. The calculated average SDs of AA 1 mM, 2 mM, 4 mM and 10 mM were 100 nm, 52 nm, 34 nm and 26 nm, respectively. The mean value of SDs were shifting to less while ammonium acetate concentration was increasing. And FWHM calculated from

histogram of AA 1 mM, 2 mM, 4 mM and 10 mM were 141 nm, 90 nm, 24 nm and 14 nm. That means 10 mM ammonium acetate buffer is useful for controllable NP array.

The density and SD of NPs changed along with change of substrate materials. With the consideration of Zeta potential or hydrophilicity, the different surface materials lead to change the SD of NPs (Fig. S2). As deposited film of Ta, Ni and Bi_2Te_3 on the substrates, the adsorption almost did not occur. For improvement of absorption, the experiment conditions were changed to form array of the PEG-ferritin. Some particular spin coater rotation speeds were found to improve the adsorption. In the experiment, at first, the spin-coater condition was designed as a group of speeds (360 rpm in 30s, 1000 rpm in 60s and 5000rpm in 30s) after incubation, the work speed at 1000rpm was established. By optimization of the spin coater condition, the NPs distribution was improved significantly. The results indicate that the adsorption of PEG-ferritin shows the same behavior even for different surface of materials.

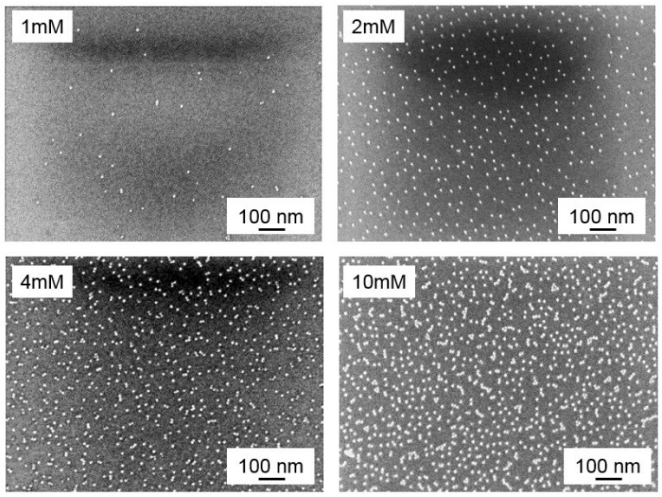

Figure S1 SEM images of PEG2k-ferritin (0.05 mg/ml) distributed on SiO_2 surface with ammonium acetate concentration of 1 mM, 2 mM, 4 mM and 10 mM.

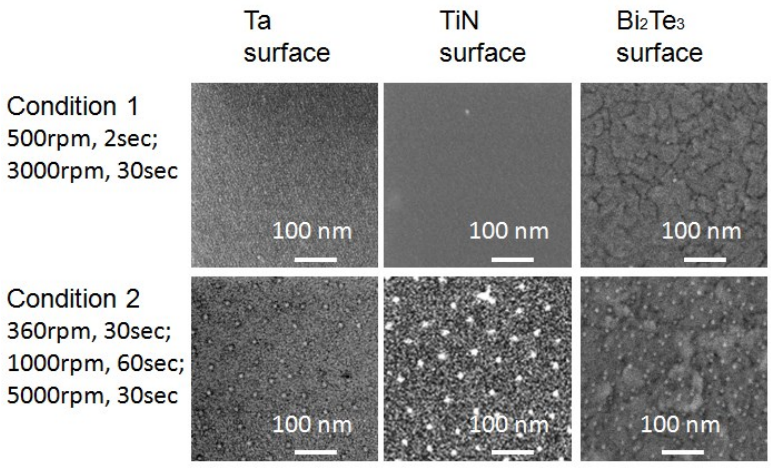

Figure S2 SEM images of PEG10k-ferritin distributed on different materials of Ta, TiN and Bi2Te3 with two spin-coater's conditions.

ACKNOWLEDGMENTS

This work was fully supported by AOARD.

REFERENCES

(1) Satoshi, S.; Yasuaki, I.; Bin, Z.; Naofumi, O.; Ichiro, Y. and Yukiharu, U. *Jpn. J. Appl. Phys.* 52, 125201 (2013).

(2) Kosuke, O.; Yukiharu, U.; Takashi, F.; Ichiro, Y.; Toshitake, Y.; Masahiro, M. and Masaki, Y. *Jpn. J. Appl. Phys.* 48, 04C153 (2009).

(3) Kaizu, T.; Tamura, Y.; Igarashi, M.; Hu, W.; Tsukamoto, R.; Yamashita, I.; Samukawa, S.; Okata, Y. *Appl. Phys. Lett.* 101,113108 (2012).

(4) Katsuhiko, K.; Shigeta, Y.; Manabu, I.; Hiroki, K.; Takanari, T.; Masatomi, S. and Masato, K. *Appl. Phys. Lett.* 101, 063103 (2012).

(5) Gojdka, B.; Hrkac, V.; Xiong, J.; Gerken, M.; Kienle, L.; Strunskus, T.; Zaporojtchenko, V. and Faupel, F. *J. Appl. Phys.* 112, 044303 (2012).

(6) Ke, Y.; Yujuan, N.; Yuanyuan, B.; Yongcun, Z. and Hong, W. *Appl. Phys. Lett.* 102, 102903 (2013).

(7) Biswas, K.; He, J.Q.; Blum, I.; Wu, C.I.; Hogan, T.P.; Seidman, D.N.; Dravid, V.P.; Kanatzidis, M. G. *Nature*, 489, 414-418 (2012).

(8) Hsu, K. F.; Loo, S.; Guo, F.; Chen, W.; Dyck, J.S.; Uher, C.; Hogan, T.; Polychroniadis, E.K.; Kanatzidis, M.G. *SCIENCE,* 303, 6, Feb. (2004).

(9) Kim, W.; Zide, J.; Gossard, A.; Klenov, D.; Stemmer, S.; Shakouri, A.; Majumdar, A. *Phys. Rev. Lett.* 96, 045901 (2006).

(10) Lin, H.; Bozin, E.S.; Billinge, S. J.L.; Quarez, E.; Kanatzidis, M.G. *Phys. Rev. B* 72, 174113 (2005).
(11) Ezzahri, Y.; Joulain, K. *J. Appl. Phys.* 113, 043510 (2013).
(12) Antonietti, M.; Göltner, C. *Angew. Chem. Int. Ed. Engl.* 36, 910-928 (1997).
(13) Feldheim, D. L.; Keating, C. D. *Chem. Soc. Rev.* 27, 1-12 (1998).
(14) Mucic, R. C.; Storhoff, J. L.; Mirkin, C. A.; Letsinger, R. L. *J. Am. Chem. Soc.* 120, 12674-12675 (1998).
(15) Klein, D. L.; Roth, R.; Kim, A. K. L.; Alivisatos, A. P.; McEuen, P. L. *Nature*, 389, 699-701 (1997).
(16) Sato, T.; Ahmed, H.; Brown, D.; Johnson, B. F. G. *J. Appl. Phys.* 82, 696-701 (1997).
(17) Sato, T.; Ahmed, H. *Appl. Phys. Lett.* 70, 2759-2761 (1997).
(18) Yabuki, S.; Mitzutani, F. *Electroanalysis* 9, 23-25 (1997).
(19) Iwahori, K.; Yoshizawa, K.; Muraoka, M.; Yamashita, I. *Inorg. Chem.* 44, 6393 (2005).
(20) Yamashita, I. *Thin Solid Film.* 393, 12 (2001).
(21) Massover, W. H. *Micron* 24, 389−437 (1993).
(22) Harrison, P. M.; Andrews, S. C.; Artymuik, P. J.; Ford, G. C.; Guest, J. R.; Hirzmann, J.; Lawson, D. M.; Livingstone, J. C.; Smith, J.M. A.; Treffry, A.; Yewdall, S. J. *Adv. Inorg. Chem.* 36, 449−486 (1991).
(23) Wong, K. K. W.; Mann, S. *Adv. Mater.* 8, 928−932 (1996).
(24) Douglas, T.; Stark, V. T. *Inorg. Chem.* 39, 1828−1830 (2000).
(25) Yamashita, I.; Hayashi, J.; Hara, M. *Chem. Lett.* 33, 1158−1159 (2004).
(26) Iwahori, K.; Yoshizawa, K.; Muraoka, M.; Yamashita, I. *Inorg. Chem.* 44, 6393−6400 (2005).
(27) Naito, M.; Iwahori, K.; Miura, A.; Yamane, M.; Yamashita, I. *Angew. Chem., Int. Edt.* 49, 7006−7009 (2010).
(28) Iwahori, K.; Takagi, R.; Kishimoto, N.; Yamashita, I. *Mater. Lett.* 65, 3245−3247 (2011).
(29) Feder, J.; Giaever, I. *J. Colloid Interface Sci.* 78, 144−154 (1980).
(30) Nygren, H. *Biophys. J.* 65, 1508−1512 (1993).
(31) Höök, F.; Rodahl, M.; Brzezinski, P.; Kasemo, B. *J. Colloid Interface Sci.* 208, 63−67 (1998).
(32) Johnson, C.A.; Yuan, Y.; Lenhoff, A.M. *J. Colloid Interface Sci.* 223, 261−272 (2000).

(33) Adamczyk, Z. *Adv. Colloid Interface Sci.* 100−02, 267−347 (2003).
(34) José M D. V.; Lorena W.; Natividad G.; Belén F.; Julio G. H. and Félix Z. *Nanotechnology* 19, 025302 (2008).
(35) Miguel, C. L.; Eugenio, C.; Alejandra, S. P.; Enrique, C.; José, M. D. V.; Natividad, G.; Rafael, M. and María, T. M. R. *Langmuir* 22 (16), pp 6993–7000 (2006).
(36) Meldrum, F.C.; Douglas, T.; Lei, S.; Arosio, P.; Mann S. *J. Inorg. Biochem.* 58, pp. 59–68 (1995).
(37) Yamashita, I.; Iwahori, K.; Kumagai, S. *Biochimica et Biophysica Acta* 1800, 846–857 (2010).
(38) Yoshizawa, K.; Mishima, Y.; Park, SY.; Heddle, JG.; Tame, JR.; Iwahori, K.; Kobayashi, M.; Yamashita, I. *J Biochem.* 142(6):707-13, Epub (2007).
(39) Zheng, B.; Yamashita, I.; Uenuma, M.; Iwahori, K.; Kobayashi, M.; Uraoka, Y. *Nanotech.* 21, 045305 (6pp) (2010).
(40) Tsukamoto, R; Godonoga, M; Matsuyama, R; Igarashi, M; Heddle, J; Samukawa, S; Yamashita, I. *Langmuir*, 29 (41), pp 12737–12743 (2013).
(41) Broyles, A. A.; Sahlin, H. L.; Carley, D. D. *Phys. Rev. Lett.* 10, 319 (1963).

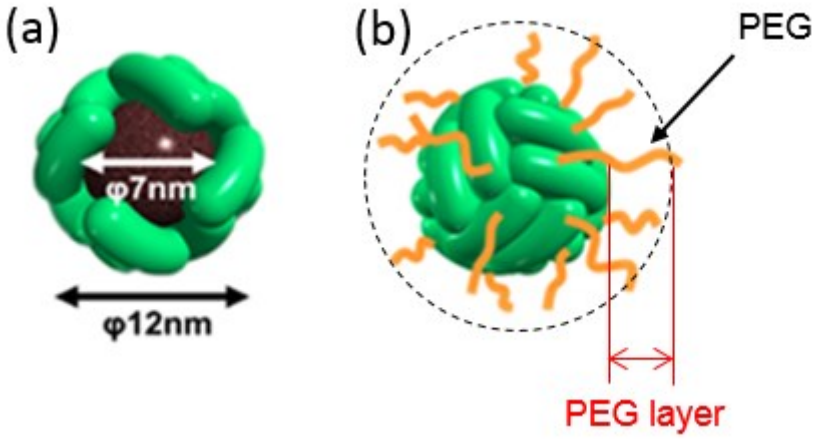

Figure 1 (a) Schematic images of ferritin protein with core and (b) PEGylated ferritin.

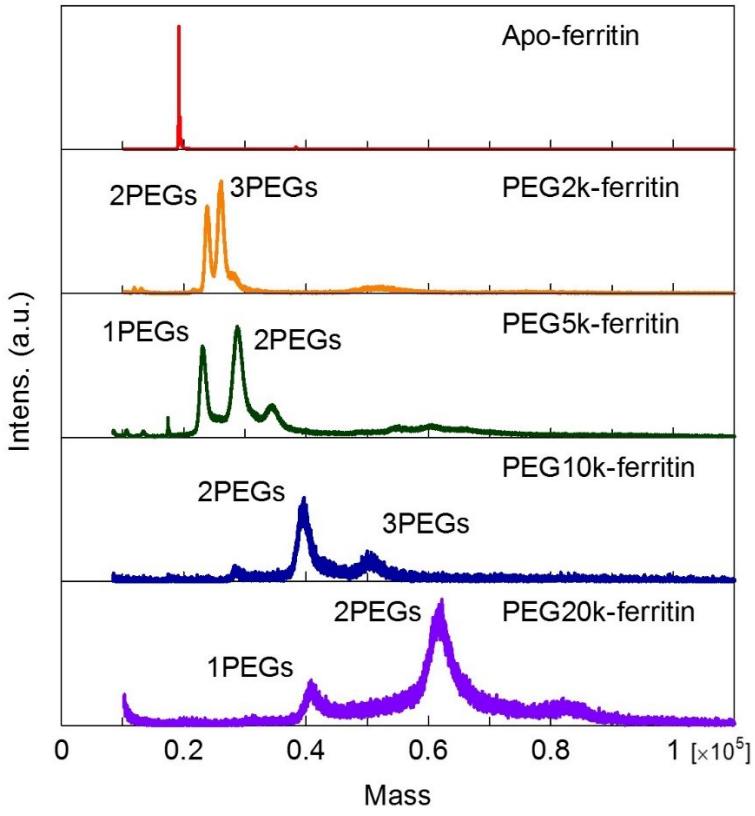

Figure 2 MALDI-TOF/MS results for analysis of ferritin (without PEG), PEG2k, 5k, 10k and 20k-ferritin.

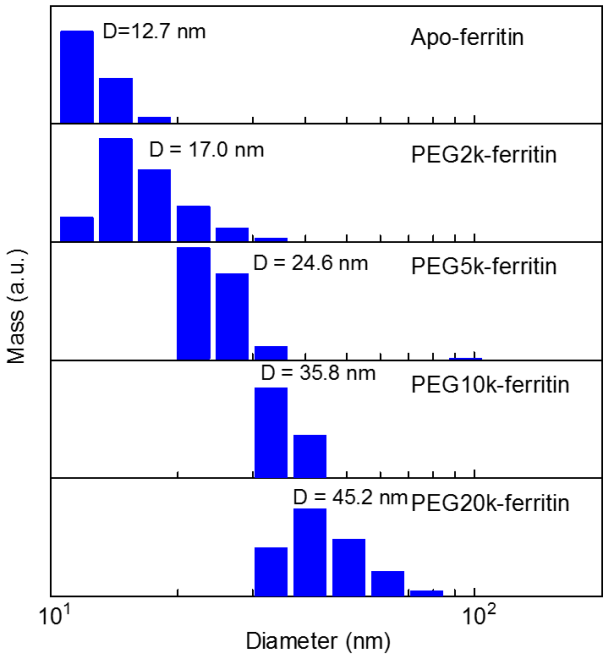

Figure 3 DLS measurement results for ferritin (without PEG), PEG2k, 5k, 10k and 20k-ferritin.

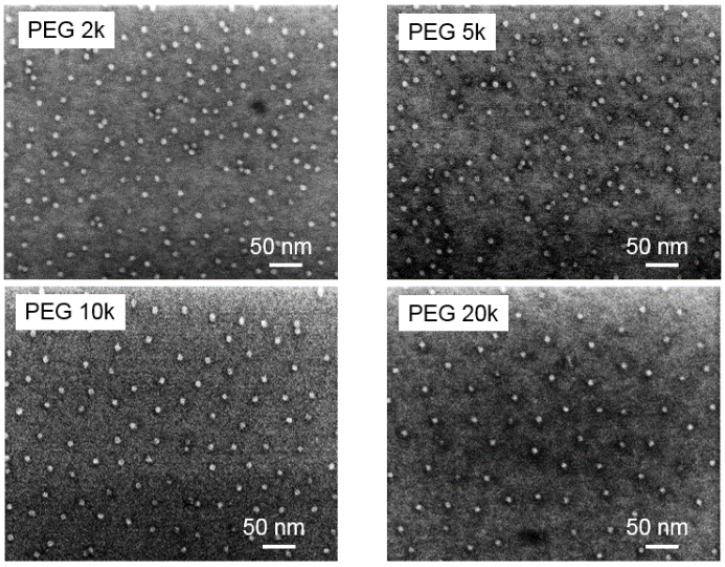

Figure 4 SEM images of PEG2k, 5k, 10k, 20k-ferritin after spin-coater process. (White dots means FeO_x core of ferritin.)

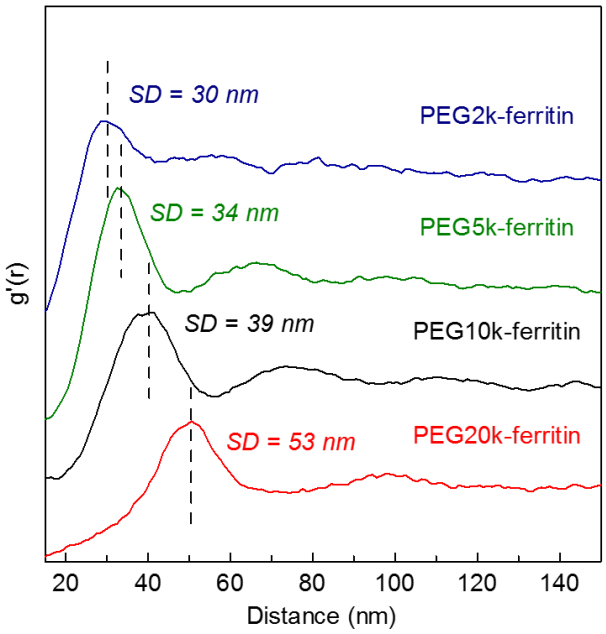

Figure 5 Calculated g'(r) of PEG-ferritin with different molecular weight of PEG.

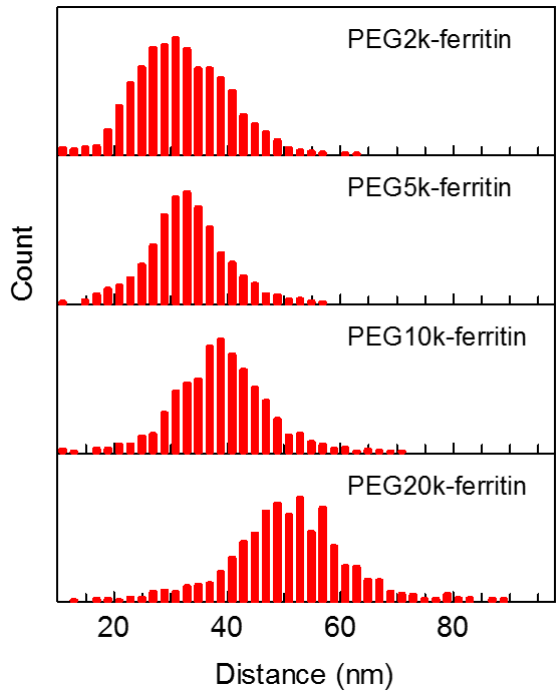

Figure 6 Calculated histograms of SD distribution in the molecular weight of PEG from 2k to 20k.

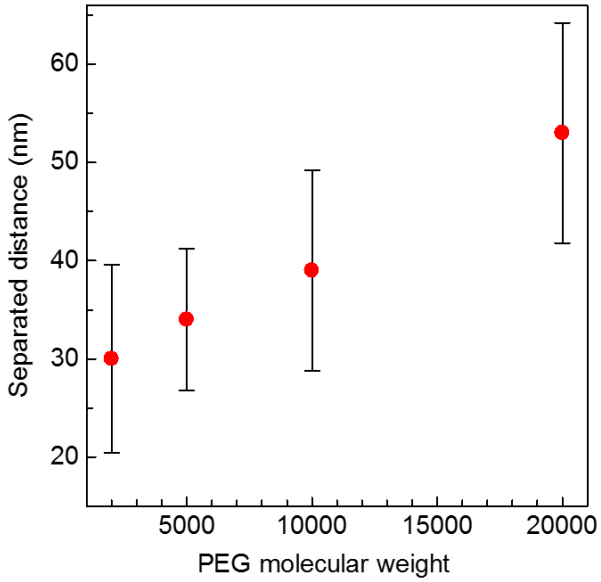

Figure 7 Relationship between PEG molecular weight and SDs.

(Red dot: calculated value from RDF; Error bar: FWHM.)

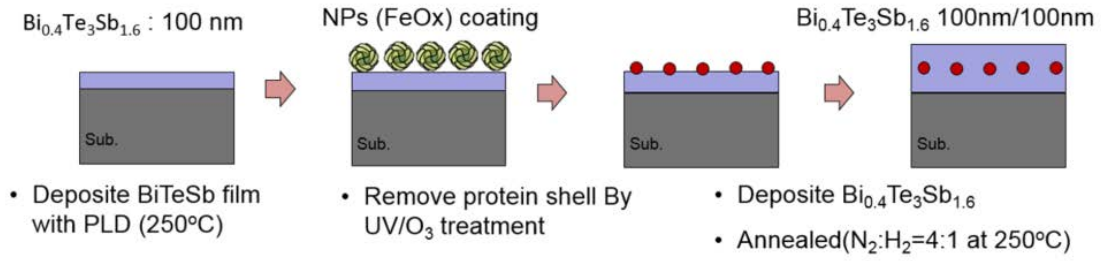

Figure 8 Deposition of BiTeSb thin film embedded with FeOx nano particle.

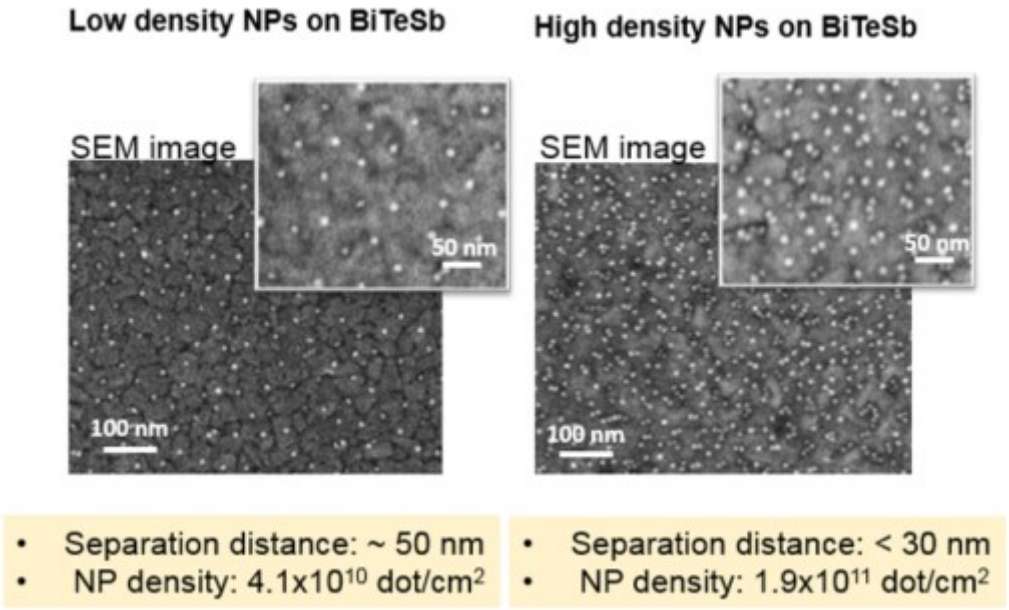

Figure 9 SEM image of the Nano particles with low density and high density on BiTeSb film

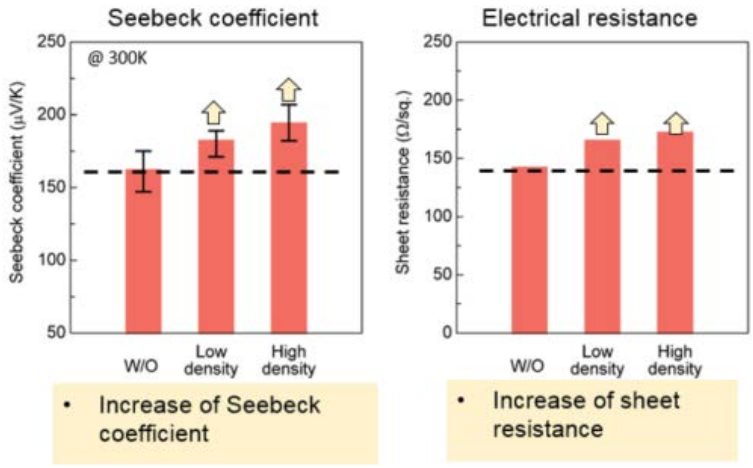

Figure 10 Seebeck coefficient and sheet resistance of BiTeSb fim with various density of nano particle. By increasing density of nano particle, seebeck coefficient greatly increased.

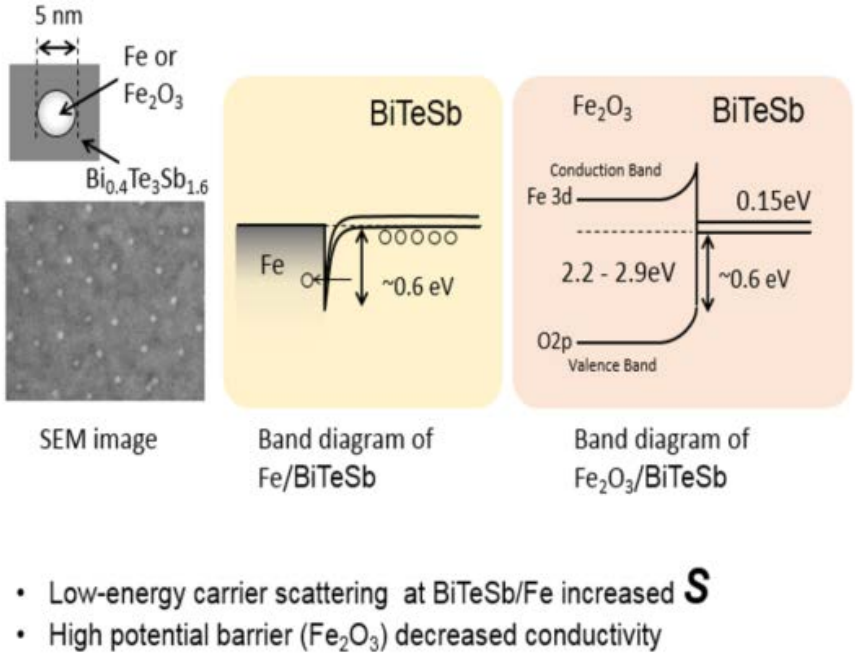

Figure 11 Energy filtering effect by the introduction of nano particle.

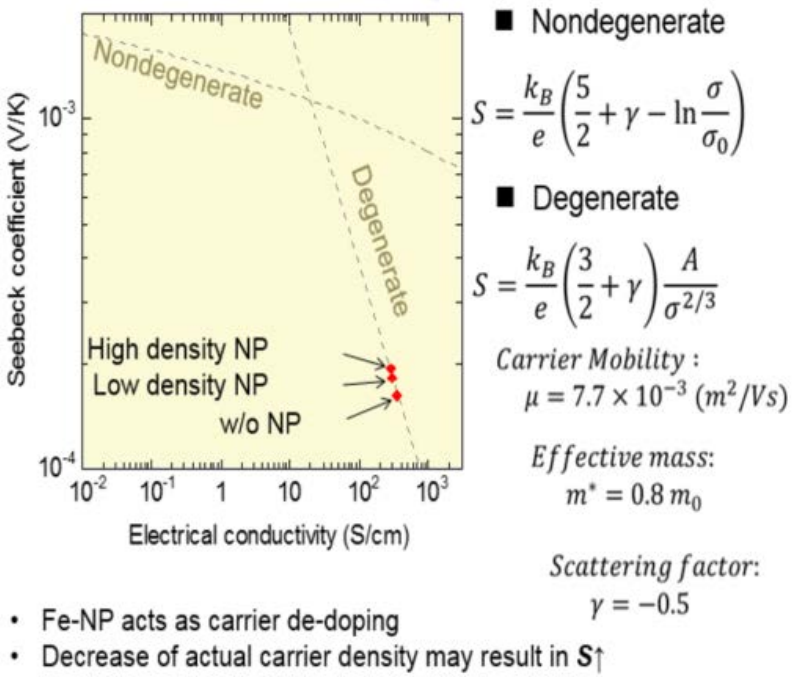

Figure 12 Effect of carrier de-doping by the introduction of nano particle.